Age Differences in Photodynamic Therapy-Mediated Opening of the Blood-Brain Barrier Through the Optical Clearing Skull Window in Mice

Chao Zhang,[1,2] Wei Feng,[1,2] Yusha Li,[1,2] Jurgen Kürths,[3,4,5] Tingting Yu,[1,2] Oxana Semyachkina-Glushkovskaya,[3]* and Dan Zhu[1,2]*

[1]*Wuhan National Laboratory for Optoelectronics-Huazhong University of Science and Technology, Britton Chance Center for Biomedical Photonics, Wuhan, Hubei 430074, China*

[2]*MoE Key Laboratory for Biomedical Photonics, Collaborative Innovation Center for Biomedical Engineering, School of Engineering Sciences, Huazhong University of Science and Technology, Wuhan, Hubei 430074, China*

[3]*Department of Physiology of Human and Animals, Saratov State University, Interdisciplinary Center of Critical Technologies in Medicine, Astrakhanskaya Str. 83, Saratov 410012, Russian Federation*

[4]*Physics Department, Humboldt University, Newtonstrasse 15, Berlin, Germany*

[5]*Potsdam Institute for Climate Impact Research, Telegrafenberg A31, Potsdam, Germany*

Background: Photodynamic therapy (PDT), a minimally invasive therapeutic tool, has been an important option for post-surgical treatment of malignant gliomas (MGs) in both adult and young patients. Recent studies have shown that PDT can also open the blood-brain barrier (BBB). However, there are no optimized parameters of PDT for patients at different ages. To determine whether there are age differences in PDT effects on the BBB, we studied PDT-related BBB opening through the optical clearing skull window in healthy 4- and 8-week-old mice.

Methods: In this work, we realized BBB opening by combining PDT with the optical clearing skull window by using different radiant exposures (635 nm, 10–20–30–40 J/cm^2) and 5-aminole-vulinic acid (5-ALA, 20 mg/kg). Then, we evaluated BBB permeability by: (i) spectrofluorimetric measuring of Evans Blue dye (EBd) leakage; (ii) confocal imaging of 70 kDa FITC-dextran extravasation and the BBB integrity; and (iii) histological analysis of brain tissues.

Results: Using the skull optical clearing method, we demonstrated PDT-induced BBB opening to EBd and FITC-dextran in a radiant exposure manner. The histological analysis revealed the different severities of vasogenic edema corresponding to radiant exposures. Besides, the PDT-related increase in the BBB permeability to high weight molecules (EBd and FITC-dextran) and solutes (vasogenic edema) was more pronounced in 4-week-old mice than in 8-week-old mice.

Conclusions: The more pronounced PDT-induced BBB disruption in juvenile mice compared with adult mice suggests age differences in PDT-related BBB opening. This might be an important informative platform for a new application of PDT as a method for brain drug delivery, especially for post-surgical treatment of MGs. Lasers Surg. Med. © 2019 Wiley Periodicals, Inc.

Key words: photodynamic therapy; blood brain barrier (BBB); optical clearing skull window; age differences

INTRODUCTION

The BBB is a highly selective barrier, which is formed by microvascular endothelial cells surrounded with pericytes and perivascular astroglia. It controls the penetration of blood-borne agents into the brain and the release of metabolites and ions from brain tissue to the blood. Therefore, BBB plays a vital role in the healthy central nervous system (CNS), protecting the brain against pathogens and toxins [1]. Although this protective mechanism is essential for a normal functioning CNS, it also creates a hindrance to the entry of drugs into the

Conflict of Interest Disclosures: All authors have completed and submitted the ICMJE Form for Disclosure of Potential Conflicts of Interest and none were reported.

Contract grant sponsor: National Natural Science Foundation of China; Contract grant numbers: 61860206009, 81870934, 31571002; Contract grant sponsor: Foundation for Innovative Research Groups of the National Natural Science Foundation of China; Contract grant number: 61721092; Contract grant sponsor: Government of the Russian Federation; Contract grant number: 14.Z50.31.0044; Contract grant sponsor: Fundamental Research Funds for the Central Universities, HUST; Contract grant number: 2018KFYXKJC026; Contract grant sponsor: Grant of Russian Science Foundation; Contract grant number: 17-15-01263; Contract grant sponsor: Director Fund of WNLO.

*Correspondence to: Oxana Semyachkina-Glushkovskaya, Department of Physiology of Human and Animals, Saratov State University, Interdisciplinary Center of Critical Technologies in Medicine, Astrakhanskaya Str. 83, Saratov 410012, Russian Federation. E-mail: glushkovskaya@mail.ru

**Correspondence to: Dan Zhu, Wuhan National Laboratory for Optoelectronics-Huazhong University of Science and Technology, Britton Chance Center for Biomedical Photonics, Wuhan, Hubei 430074, China. E-mail: dawnzh@mail.hust.edu.cn

Accepted 29 January 2019

Published online 27 February 2019 in Wiley Online Library (wileyonlinelibrary.com).

DOI 10.1002/lsm.23075

brain [2,3]. This is the reason why approaches for reversible overcoming of the BBB have received significant attention in the last four decades [4–6].

In our previous studies on adult mice, we demonstrated that PDT temporally increases BBB permeability [7,8]. Our results are consistent with data of Hirschberg et al. and Madsen et al., who also showed PDT-related BBB opening using a 400 μm bare flat-end quartz fiber (635 nm) with 5-ALA and 670 nm laser application with aluminum phthalocyanine disulfonate (AlPcS2a) [9–11].

These novel data related to PDT-induced BBB opening warrant revision of our knowledge about the cerebrovascular effects of PDT and will stimulate the development of novel therapeutic applications of PDT, such as brain drug delivery in post-surgical PDT of MGs, which is distinct in both children and adults.

Histologically, the pediatric MGs (PMGs) and adult MGs (AMGs) are similar. However, there are quite different biological, genetic, and molecular characteristics of MGs in these two populations [12,13]. The PMGs are characterized by a more aggressive clinical behavior than AMGs. As compared to AMGs, PMGs seem to possess a statistically higher incidence of chromosomal mutations, such as gains at 1q and losses at 16q and 4q [14–20]. Mutations in the p53 pathway are much more common in PMGs [21,22]. Many abnormalities identified in AMGs, such as retinoblastoma gene mutation and amplifications of the MYC, MYCN, CDK6, CCND2, and PTEN mutations, are less prevalent among PMGs [12,13,21,23]. The expression of oncological molecular factors, such as platelet-derived growth factor receptor A, is predominant in PMGs, while a high expression of the epidermal growth factor receptor is more common in AMGs [12,13,16,24,25].

The mechanisms of the BBB functioning in fetuses and in early stages of ontogeny are different from those in adults [26]. In embryonic development, tight junctions appear early, restricting the entrance of proteins into the brain [27]. The expression of ABC-influx/efflux transporters during mid-gestation is even higher than in adults [28]. At birth, the BBB is functional with no fenestrations [29], but the gene expression of BBB endothelial proteins undergoes changes in normal brains from the postnatal period to adulthood [30]. In our previous study, we demonstrated a greater expression of the two main tight junction proteins of the BBB (occludin and claudin-5) in neonatal versus adult rats [31].

However, despite clear age differences in MG etiology and BBB functions, there are no accepted standards of care and treatment of MGs with age-related algorithms. Historically, the therapy of MGs was simply adopted from AMGs to PMGs. Nowadays, due to a better understanding of age differences in MG biology, it has become clear that these strategies may not be the most effective solution to achieve advances in the treatment of PMGs. Therefore, the development of new advances in technologies and methods for therapy of MGs with age-related approaches is a challenging task.

Since PDT is one of the most promising therapeutic approaches in post-surgical treatment of both PMGs and AMGs, for a better understanding of age differences in the cerebrovascular effects of PDT, we studied PDT-mediated opening of the BBB in a radiant exposure manner (635 nm, 10–20–30–40 J/cm^2 and 5-ALA, 20 mg/kg) in healthy 4- and 8-week-old mice by using quantitative and qualitative tests for BBB permeability. Additionally, we analyzed age differences of PDT on the brain tissues using a histological method. To enhance the light penetration through the skull and avoid or significantly decrease negative influences of PDT on BBB permeability, we performed PDT through the optical clearing skull window.

MATERIALS AND METHODS

Subjects

Experiments were carried out on Balb/c mice (4 and 8 weeks, male). The animals were divided into control and PDT treatment groups. The control groups include: (i) without PDT treatment; (ii) 5-ALA injection without laser irradiation; and (iii) laser irradiation without 5-ALA injection. The PDT treatment groups were divided into 16 sub-groups corresponding with different ages (4- and 8-week-old mice), radiant exposures (10, 20, 30, and 40 J/cm^2), and time of BBB opening and recovery (1.5 and 4 hours after PDT). $n = 6$ mice in each group and subgroup, and all the mice were treated by skull optical clearing agent.

All experimental protocols were performed according to the Experimental Animal Management Ordinance of Hubei Province, P. R. China, and the guidelines from the Huazhong University of Science and Technology, which have been approved by the Institutional Animal Ethics Committee of Huazhong University of Science and Technology.

Protocol of BBB Opening Through the Optical Clearing Skull Window by PDT

The mice were anesthetized with a cocktail of 2% α-chloralose and 10% urethane (8 mg/kg) via intraperitoneal injection. The head was shaved and a midline incision was made on the scalp. Then the scalp was removed and the skull surface was dried by clean compressed air. After that, we used skull optical clearing agents to establish an optical clearing skull window (diameter: 5 mm). The detailed descriptions about preparation and application method of skull optical clearing agents are reported in reference [32].

The PDT was performed 30 minutes after intravenous injection of 5-ALA (20 mg/kg) according to previous studies [7,8]. We measured the irradiance of the laser by a photosensor that was placed on the front surface of a cranial bone, and it was irradiated from a 5-mm distance with a laser diode (LD) light source at the wavelength of 635 nm (NJL-LD-635-5-F-R, China, bandwidth: 3 nm, diameter of the beam: 2 mm, Gaussian's beam profile). Various radiant exposures of 10, 20, 30, and 40 J/cm^2 were achieved by using constant irradiance at 165 mW/cm^2 for durations of 1, 2, 3, and 4 minutes, respectively.

Assessment of the BBB Permeability

To evaluate the BBB permeability, we used three different methods.

(1) The first test was a spectrofluorometric assay of Evans Blue dye (EBd) extravasation. The EBd (Sigma Chemical Co., St. Louis, MI) was injected in a single bolus dose (2 mg/25 g, 1% solution in physiological 0.9% saline) and circulated for 30 minutes in the blood. The EBd injection was performed 60 or 210 minutes after PDT. At the end of the circulation time (30 minutes), the mice were decapitated, and their brains were rapidly collected and placed on ice. The EBd extraction and visualization were performed according to Wang et al. [33].
(2) The second test used confocal microscopy to detect FITC-dextran extravasation. In brief, 70 kDa FITC-dextran (Sigma Chemical Co.) was injected intravenously (4 mg/25 g, 0.5% solution in 0.9% physiological saline) 88 minutes after PDT treatment and circulated for 2 minutes. Afterwards, mice were decapitated and their brains were rapidly removed and fixed in 4% paraformaldehyde (PFA) for 24 hours. The brains were cut into 100-μm thick slices on a vibratome (Leica VT 1000S Microsystem, Germany) and analyzed on a confocal microscope (A1R, Nikon, Japan). Approximately 8–12 slices per animal from cortical and subcortical (except hypothalamus and choroid plexus where the BBB is leaky) regions were imaged. Then the BBB permeability was evaluated in groups [34]. The dextran extravasation was determined as clear specific fluorescence occurring outside of the vessel walls and was classified as weak (+), medium (++), strong (+++), and diffusive (++++). Weak infiltration was defined as a faint cloud, clearly associated with one vessel site of the tracer leakage. Medium was defined as a bright cloud, clearly associated with one vessel site of the tracer leakage. Strong extravasation was defined as a bright cloud clearly associated with a group of vessels. Diffusive extravasation was defined as extensive leakage of the tracer in many places of the brain without clear association with specific vessels.
(3) The third test was a histological analysis of the BBB permeability to solutes. Mice were decapitated 1.5 hours after PDT. The samples were fixed in 4% PFA for 24 hours. Then the fixed specimens were embedded in paraffin, sectioned (4 μm) and stained with haematoxylin and eosin. The histological sections were evaluated by an upright microscope system (Nikon, Japan).

To evaluate the integrity of the neurovascular unit (NVU), we detected three different indicators: (i) the endothelial barrier antigen conjugated with antibodies SMI-71; (ii) the anti-glial fibrillary acidic protein (GFAP) labeling astrocytes; and (iii) the laminin, labeling the basal lamina membranes.

The preparation of the brain slices was the same as that in the second test. Afterwards, the brains were fixed in 4% PFA and cut into 100-μm thick slices with further permeabilization with PBS containing 0.2‰ Triton-X-100 (Sigma–Aldrich) for 30 minutes. Then potential nonspecific binding sites were blocked with 5% bovine serum albumin (BSA, Sigma–Aldrich) for 45 minutes at room temperature. After that, the slices were incubated with the primary antibody (SMI-71: 1:200; GFAP: 1:200; laminin: 1:40) at 4°C overnight. After being washed, the sections were then incubated with secondary antibodies (1:500) for 1 hour at room temperature. Finally, the slices were imaged by confocal microscope (A1R, Nikon).

Statistical Analysis

In this work, all data are expressed as mean ± standard error unless stated otherwise. Significant differences were analyzed using one-way analysis of variance test with SPSS (IBM, Chicago, IL).

RESULTS

PDT-Induced Opening of BBB Evaluated by Assessing EBd Extravasation

Next, we investigated PDT-induced changes in the BBB permeability to the EBd albumin complex using spectrofluorimetric assay in 4- and 8-week-old mice. EBd, a commonly-used 961 kDa dye that binds to serum albumin forming high weight molecules, cannot permeates the intact BBB, thus, its leakage into brain tissue is widely used to evaluate BBB disruption.

The BBB permeability to EBd was analyzed every 30 minutes after 5-ALA-mediated PDT over a 4 hours duration. Here, we presented two time points: 90 minutes after PDT, when we observed the first significant changes in the BBB; and 4 hours after PDT, when we did not see further increases in the leakage of EBd.

The results are presented in Table 1. There were no changes in BBB permeability to the EBd albumin complex in mice of both ages in all groups, including laser irradiation itself or 5-ALA injection without laser as well as in the untreated mice.

However, we found significant age differences in PDT-related opening of the BBB to EBd. Indeed, an increase in BBB permeability to EBd induced by radiant exposures of 10 and 20 J/cm^2 was 1.7 and 1.6 times higher in 4-week-old mice compared with 8-week-old ones (Table 1). However, application of higher radiant exposures (30 and 40 J/cm^2) was accompanied by a significant EBd leakage that was similar for both ages.

Four hours after PDT, the content of EBd in the brain for both 4- and 8-week-old mice with different radiant exposures returned to the normal state, suggesting the BBB recovery.

Thus, this series of experiments clearly demonstrate age differences in PDT-mediated opening of the BBB when low radiant exposures (10 and 20 J/cm^2) were applied. However, high radiant exposures (30 and 40 J/cm^2) induced comparable BBB disruption for both ages.

TABLE 1. The PDT-Related Changes in the BBB Permeability to EBd

Groups		Content of Evans Blue in the brain (μg/g tissue)		
Age		4 weeks		8 weeks
Control (with optical clearing skull window)				
Untreated mice		0.60 ± 0.01 ($n = 6$)		0.69 ± 0.01 ($n = 6$)
5-ALA		0.64 ± 0.03 ($n = 6$)		0.66 ± 0.01 ($n = 6$)
Laser 10 J/cm^2		0.59 ± 0.01 ($n = 6$)		0.62 ± 0.02 ($n = 6$)
Laser 20 J/cm^2		0.62 ± 0.02 ($n = 6$)		0.61 ± 0.01 ($n = 6$)
Laser 30 J/cm^2		0.60 ± 0.01 ($n = 6$)		0.65 ± 0.03 ($n = 6$)
Laser 40 J/cm^2		0.64 ± 0.02 ($n = 6$)		0.67 ± 0.03 ($n = 6$)
Time	1.5 hours after PDT	4 hours after PDT	1.5 hours after PDT	4 hours after PDT
PDT (635 nm + 5-ALA (with optical clearing skull window)				
Laser 10 J/cm^2	11.24 ± 0.50 ($n = 6$) *†	0.66 ± 0.06 ($n = 6$)	7.62 ± 0.50 ($n = 6$) *	0.62 ± 0.09 ($n = 6$)
Laser 20 J/cm^2	19.19 ± 1.05 ($n = 6$) *†	0.67 ± 0.04 ($n = 6$)	13.86 ± 0.71 ($n = 6$) *	0.66 ± 0.08 ($n = 6$)
Laser 30 J/cm^2	18.98 ± 1.21 ($n = 6$) *	0.63 ± 0.06 ($n = 6$)	18.02 ± 1.17 ($n = 6$) *	0.69 ± 0.05 ($n = 6$)
Laser 40 J/cm^2	18.85 ± 1.10 ($n = 6$) *	0.71 ± 0.06 ($n = 6$)	18.30 ± 1.47 ($n = 6$) *	0.65 ± 0.04 ($n = 6$)

$P < 0.05$: *- versus the untreated mice group; †- versus between two age groups.

Qualitative Evaluation of PDT-Induced Opening of the BBB

The above quantitative data from spectrofluorimetric assay of EBd complex content in brain tissue can accurately reflect the changes in BBB permeability after PDT, but the coloration of the brain tissues cannot be directly viewed. Here, we have a guideline for evaluating BBB permeability by injection of dextran (70 kDa) and qualitatively characterizing the figures [34]. Therefore, in the second series of experiments, we tested the PDT-related opening of the BBB by confocal imaging of FITC-dextran extravasation (Fig. 1).

Figure 1 shows direct viewings of FITC leakages in different conditions, and we outlined the vessels profiles in the magnified maps. Results shows that there is no FITC-dextran leakage in the control groups. Radiant exposure of 10 and 20 J/cm^2 caused strong FITC-dextran extravasation for 4-week-old mice (bright cloud associated with a groups of vessels), but for 8-week-old mice, it was weak (a faint cloud around one vessel) at 10 J/cm^2 and medium (a bright cloud around one vessel) at 20 J/cm^2. As for high radiant exposures, it accompanied by diffuse type of FITC-dextran extravasation for both age groups of mice.

These results with the usage of confocal imaging of FITC-dextran extravasation clearly show that PDT-related opening of the BBB depends on radiant exposures and age of mice. For low and medium radiant exposures (10–20 J/cm^2), 4-week-old mice demonstrate more significant changes in BBB permeability to FITC-dextran compared with 8-week-old mice, while high radiant exposures (30–40 J/cm^2) causes significant BBB disruption in both age groups (Table 2).

Changes in BBB Structure Integrity After PDT

Figure 2 shows the confocal imaging of PDT-induced BBB opening to FITC-dextran using specific markers of NVU at radiant exposures of 10 and 20 J/cm^2 for 4- and 8-week-old mice. Figure 2A demonstrates FITC-dextran leakage outside of the endothelial cells of cerebral vessels labeled by SMI. Figure 2B demonstrates FITC-dextran leakage outside the basal membrane labeled by the antibodies of laminin, which is one of the proteins of the basal membrane. Figure 2C illustrates the FITC-dextran extravasation from the cerebral vessels into the brain tissues among astrocytes.

These experimental data clearly exhibit that the selected tracer of FITC-dextran effectively crossed all elements of the BBB, including the cerebral endothelium, the basal membrane and astrocytes after PDT.

Morphological Evaluation of PDT-Induced Opening of the BBB

To analyze the morphological changes in the brain tissues and cerebral vessels after PDT using different radiant exposures, we performed histological studies in mice of both ages.

Figure 3 uncovers that the PDT-mediated opening of BBB was accompanied by the formation of vasogenic edema (the empty area around vessels) in a radiant exposure-dependent manner: for higher radiant exposures, a more extravasated volume of extensive solutes was observed around the cerebral microvessels. It is important to emphasize that these changes were more pronounced in juvenile mice compared with adult ones.

DISCUSSION

Our results clearly demonstrate that PDT causes a radiant exposure-dependent increase in BBB permeability to high weight molecules such as EBd (68.5 kDa) and FITC dextran (70 kDa) for both ages of mice. Up to now, the mechanisms underlying PDT-mediated opening of the BBB have not been revealed completely. Some reports stated that PDT has effects

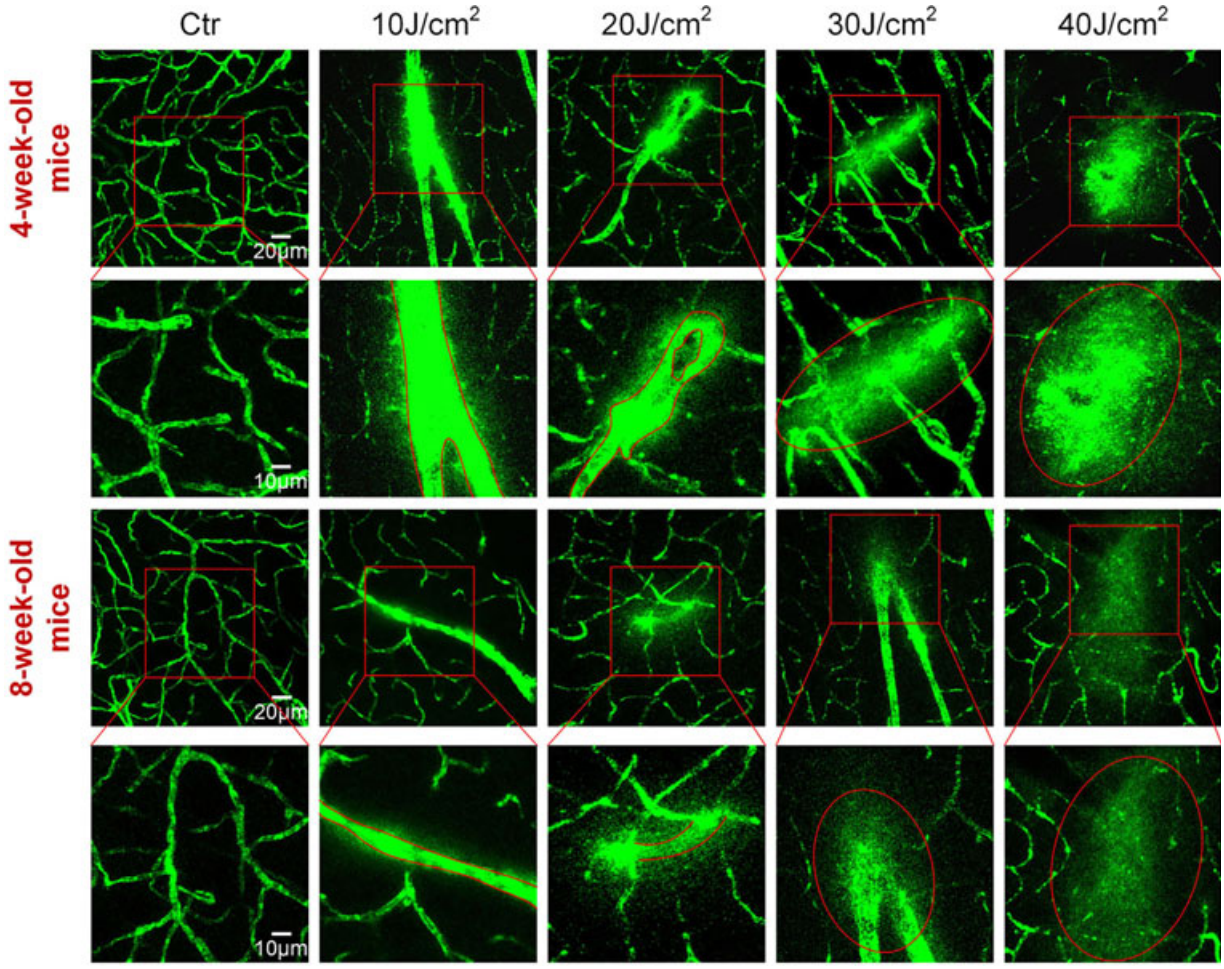

Fig. 1. The PDT-related opening of the BBB evaluated by confocal imaging of FITC-dextran (70 kDa) extravasation from cerebral vessels into the brain parenchyma. In each group, images in second rows are magnified maps of the area enclosed in the first row, and the profiles of vessels are outlined.

on the endothelial cells resulting in increasing gaps between endothelial cells via changes of the cytoskeleton, cell rounding, and constriction loss due to microtubule depolarization [35–38]. The singlet oxygen ($^1O_2$) generated during PDT causes endothelial regulation imbalance of vascular relaxation. Thus, the vascular resistance to photo-induced oxidative stress decreases, resulting in the redistribution of calcium, reduction of influx, and calcium release from intracellular storage [39–42]. In our study, using markers of NVU such as SMI (the vascular endothelial cells), laminin (the basal membrane), and GFAP (the astrocytes), we uncovered disorders of NVU resulting in an increase of BBB permeability. Therefore, the tested tracer (dextran, 70 kDa) passed through the vascular endothelium and the basal membrane with further distribution between astrocytes.

Our data also demonstrate that there are age differences in PDT-related opening of the BBB. The cerebral vessels of 4-week-old mice are more sensitive to PDT-mediated changes in the BBB permeability compared with 8-week-old mice. The young mice demonstrated a more significant increase in the leakage of EBd and 70 kDa FITC-dextran after application of low and medium radiant exposures (10–20 J/cm^2).

The age-related differences in PDT-mediated opening of the BBB can be related to BBB maturation,

TABLE 2. PDT-Related Opening of BBB Evaluated by FITC-Dextran Extravasation

Radiant exposures	Classification of FITC-dextran extravasation	
Age	4 weeks	8 weeks
Control (with optical clearing skull window)($n = 6$)	/	/
10 J/cm^2 ($n = 6$)	+++ (*)	+
20 J/cm^2 ($n = 6$)	+++ (*)	++
30 J/cm^2 ($n = 6$)	++++	++++
40 J/cm^2 ($n = 6$)	++++	++++

/: normal; +: weak; ++: medium; +++: strong; ++++: diffuse.
*- between two age groups.

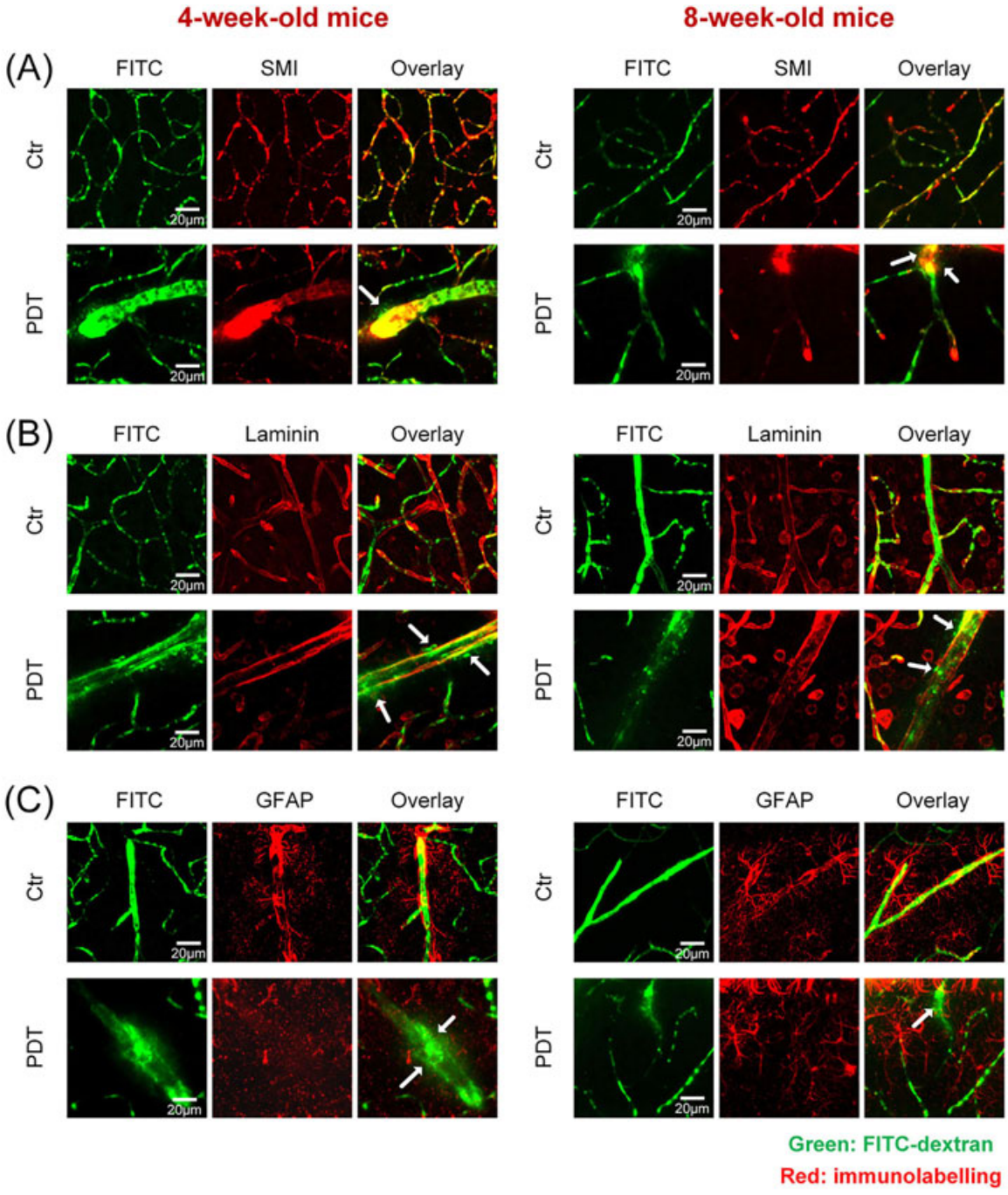

Fig. 2. The confocal imaging of PDT-induced opening of the BBB to FITC-dextran using specific markers of NVU: (**A**) FITC-dextran leakage outside of the endothelial cells of cerebral vessels labeled by SMI; (**B**) FITCdextran leakage outside the basal membrane labeled by the antibodies for the laminin; (**C**) FITC-dextran extravasation from the cerebral vessels into the brain tissues among astrocytes. The white arrows points to the sites of FITC-dextran leakage.

which continues after birth. The BBB restricts the entrance of proteins into the brain that already exists in fetuses [26,27]. It is interesting to note that the expression of the ABC-influx/efflux transporters during mid-gestation is higher than in adults [28]. At birth, the expression of two main tight junction proteins of BBB (occludin and claudin-5) is higher in newborn rats than in adult rats and the BBB has no fenestrations [29,31]. In other stages of ontogeny, the gene expression of BBB endothelial proteins undergoes changes in a normal brain from the postnatal period to adulthood [30].

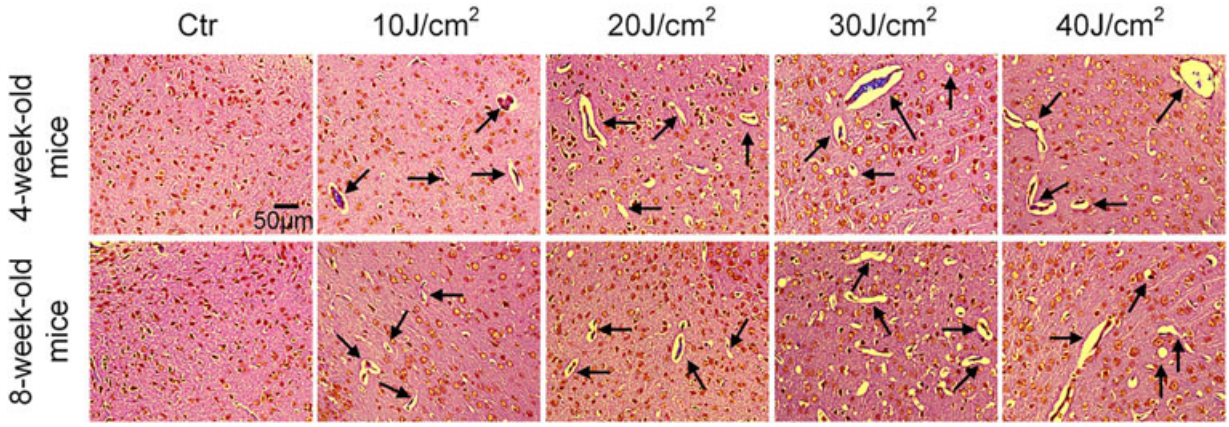

Fig. 3. PDT-induced opening of the BBB evaluated by histological analysis of solute extravasation in 4- and 8-week-old mice. Ctr—the control group, where there was no solute leakage; 10, 20, 30, and 40 J/cm2 caused the perivascular edema (black arrows), which appears as empty spaces around cerebral vessels.

Thus, the BBB maturation might be a crucial reason for age differences in PDT-mediated opening of the BBB, which is decisive for optimization of guidelines of PDT-treatment of MGs in young and adult patients.

Our results also demonstrate that PDT-mediated opening of the BBB is accompanied by the development of vasogenic edema, which is more pronounced in young mice than in adult mice. The formation of vasogenic edema after PDT has also been shown in other works using 5-ALA [10,43,44]. One of the mechanisms responsible for an extensive fluid accumulation in the perivascular space of the brain is disruption of the tight junction complex and imbalance in the control of expression of the aquaporin channels in the astrocytes and the vascular endothelium [45,46].

The PDT-mediated opening of the BBB is accompanied by activation of the meningeal lymphatics, which play a major role in brain clearing of molecules that crossed the opened BBB [47]. The activation of lymphatic drainage contributes to the elimination of water from the extracellular space and recovery of fluid balance in the brain. In our serial works, we clearly show the recruitment of the meningeal lymphatics by BBB opening, including PDT-mediated opening of the BBB [48].

There are age differences in the development of the meningeal lymphatics and in the brain drainage system. The meningeal lymphatic system develops postnatally and becomes fully anatomically present by day 28 of ontogeny [49]. However, there is no information about the functional development of the meningeal lymphatic system. It is well known that the arachnoid elements that absorb brain fluids into the venous system do not exist prenatally. They become visible in infants, but only exist in abundance in adults [50,51].

These facts allow us to assume that the more significant PDT-related vasogenic edema in young mice versus adult mice can be explained by the undeveloped brain drainage system and meningeal lymphatic vessels.

Note that high radiant exposure (40 J/cm^2) caused severe vasogenic edema after PDT for both young and adult mice. This fact suggests that high radiant exposure induces BBB disruption beyond the brain reserve capability, which agrees with our previous results [7].

In this work, another important approach for minimizing negative consequences of PDT effects to the brain vasculature and tissues is the application of the skull optical clearing technique [32,52,53]. Generally, PDT performance requires a craniotomy in both clinical and fundamental studies due to the high scattering property of the skull, which leads to low light penetration into the brain [7,9,10,54–56]. However, the craniotomy leads to brain swelling, increasing in intracranial pressure and cortical inflammation [10]. Our results clearly demonstrate that the newly-developed skull optical clearing technique assists us to realize BBB opening by PDT without craniotomy. By applying this method, we demonstrate the effective application of PDT through the skull with low doses of laser and photosensitizer, and demonstrate the possibility of using PDT for modulating BBB permeability.

CONCLUSIONS

In summary, our findings presented a novel understanding about age differences in PDT-mediated opening of the BBB. Young mice demonstrated a more pronounced PDT-induced increase in BBB permeability to high weight molecules (EBd 68.5 kDa and dextran 70 kDa) as well as to solutes which were observed as vasogenic edema.

These data are an important informative platform for a new application of PDT as a method for brain drug delivery, especially in post-surgical treatment of MGs. We also believe that the skull optical clearing technique will be an effective method for PDT application through the intact skull in mice, which will be an important strategy for brain drug delivery and brain diseases therapy.

ACKNOWLEDGMENTS

This work was supported by National Natural Science Foundation of China (NSFC) (Grant Nos. 61860206009, 81870934, 31571002, 81701354); the Foundation for

Innovative Research Groups of the National Natural Science Foundation of China (Grant No. 61721092); the Grant of Russian Science Foundation (Grant No. 17-15-01263); the Fundamental Research Funds for the Central Universities, HUST (No. 2018KFYXKJC026); Government of the Russian Federation (Grant No. 14. Z50.31.0044), and Director Fund of WNLO. We also thank the Optical Bioimaging Core Facility of WNLO for support in data acquisition.

REFERENCES

1. Abbott NJ, Patabendige AAK, Dolman DEM, Yusof SR, Begley DJ. Structure and function of the blood-brain barrier. Neurobiol Dis 2010;37(1):13–25.
2. Pardridge WM. Molecular Trojan horses for blood-brain barrier drug delivery. Discov Med 2006;6(34):139–143.
3. Ghose AK, Viswanadhan VN, Wendoloski JJ. A knowledge-based approach in designing combinatorial or medicinal chemistry libraries for drug discovery. 1. A qualitative and quantitative characterization of known drug databases. J Comb Chem 1999;1(1):55–68.
4. Hammarlund-Udenaes M, Lange ECMD, Thorne RG. Drug delivery to the brain: Physiological concepts, methodologies and approaches. Curr Drug Deliv 2017;15(3).
5. Mitragotri S. Devices for overcoming biological barriers: The use of physical forces to disrupt the barriers. Adv Drug Deliver Rev 2013;65(1):100–103.
6. Pandey PK, Sharma AK, Gupta U. Blood brain barrier: An overview on strategies in drug delivery, realistic *in vitro* modeling and *in vivo* live tracking. Tissue Barriers 2016;4(1): e1129476.
7. Semyachkina-Glushkovskaya O, Kurths J, Borisova E, et al. Photodynamic opening of blood-brain barrier. Biomed Opt Express 2017;8(11):5040–5048.
8. Zhang C, Feng W, Vodovozova E, et al. Photodynamic opening of the blood-brain barrier to high weight molecules and liposomes through an optical clearing skull window. Biomed Opt Express 2018;9(10):4850–4862.
9. Madsen SJ, Hirschberg H. Site-specific opening of the blood-brain barrier. J Biophotonics 2010;3(5–6):356–367.
10. Hirschberg H, Uzal FA, Chighvinadze D, Zhang MJ, Peng Q, Madsen SJ. Disruption of the blood-brain barrier following ALA-mediated photodynamic therapy. Lasers Surg Med 2008;40(8):535–542.
11. Madsen SJ, Gach HM, Hong SJ, Uzal FA, Peng Q, Hirschberg H. Increased nanoparticle-loaded exogenous macrophage migration into the brain following PDT-induced blood-brain barrier disruption. Lasers Surg Med 2013;45(8):524–532.
12. Fangusaro J. Pediatric high grade glioma: A review and update on tumor clinical characteristics and biology. Front Oncol 2012;2:105–105.
13. Jones C, Perryman L, Hargrave D. Paediatric and adult malignant glioma: Close relatives or distant cousins? Nat Rev Clin Oncol 2012;9(7):400–413.
14. Schiffman JD, Hodgson JG, VandenBerg SR, et al. Oncogenic BRAF mutation with CDKN2A inactivation is characteristic of a subset of pediatric malignant astrocytomas. Cancer Res 2010;70(2):512–519.
15. Wong KK, Tsang YTM, Chang YM, et al. Genome-wide allelic imbalance analysis of pediatric gliomas by single nucleotide polymorphic allele array. Cancer Res 2006;66(23):11172–11178.
16. Paugh BS, Qu C, Jones C, et al. Integrated molecular genetic profiling of pediatric high-grade gliomas reveals key differences with the adult disease. J Clin Oncol 2010;28(18): 3061–3068.
17. Schwartzentruber J, Korshunov A, Liu XY, et al. Driver mutations in histone H3.3 and chromatin remodelling genes in paediatric glioblastoma. Nature 2012;482(7384):226–231.
18. Barrow J, Adamowiczbrice M, Cartmill M, et al. Homozygous loss of ADAM3A revealed by genome-wide analysis of pediatric high-grade glioma and diffuse intrinsic pontine gliomas. Neuro-Oncol 2011;13(2):212–222.
19. Qu HQ, Jacob K, Fatet S, et al. Genome-wide profiling using single-nucleotide polymorphism arrays identifies novel chromosomal imbalances in pediatric glioblastomas. Neuro-Oncol 2010;12(2):153–163.
20. Bax DA, Mackay A, Little SE, et al. A distinct spectrum of copy number aberrations in pediatric high-grade gliomas. Clin Cancer Res 2010;16(13):3368–3377.
21. Rood BR, MacDonald TJ. Pediatric high-grade glioma: Molecular genetic clues for innovative therapeutic approaches. J Neuro-Oncol 2005;75(3):267–272.
22. Pollack IF, Finkelstein SD, Woods J, et al. Expression of p53 and prognosis in children with malignant gliomas. New Engl J Med 2002;346(6):420–427.
23. Broniscer A, Gajjar A. Supratentorial high-grade astrocytoma and diffuse brainstem glioma: Two challenges for the pediatric oncologist. Oncologist 2004;9(2):197–206.
24. Libermann TA, Nusbaum HR, Razon N, et al. Amplification, enhanced expression and possible rearrangement of EGF receptor gene in primary human brain tumours of glial origin. Nature 1985;313(5998):144–147.
25. Ii FGB, Simmons ML, Chang SM, et al. EGFR overexpression and radiation response in glioblastoma multiforme. Int J Radiat Oncol 2001;51(2):410–418.
26. Saunders NR, Habgood MD, Dziegielewska KM. Barrier mechanisms in the brain, II. Immature brain. Clin Exp Pharmacol P 1999;26(2):85–91.
27. Kniesel U, Risau W, Wolburg H. Development of blood-brain barrier tight junctions in the rat cortex. Dev Brain Res 1996;96(1–2):229–240.
28. Ek CJ, Wong A, Liddelow SA, Johansson PA, Dziegielewska KM, Saunders NR. Efflux mechanisms at the developing brain barriers: ABC-transporters in the fetal and postnatal rat. Toxicol Lett 2010;197(1):51–59.
29. Engelhardt B. Development of the blood-brain barrier. Cell Tissue Res 2003;20(6):119–129.
30. Richard D, Lu Z, Amanuel AK, Ben AB. Pericytes are required for blood-brain barrier integrity during embryogenesis. Nature 2010;468(7323):562–566.
31. Semyachkina-Glushkovskaya O, Sindeeva O, Abdurashitov A, et al. Blood-brain barrier and cerebral blood flow: Age differences in hemorrhagic stroke. J Innov Opt Heal Sci 2015;8(6):1550045.
32. Zhang C, Feng W, Zhao Y, et al. A large, switchable optical clearing skull window for cerebrovascular imaging. Theranostics 2018;8(10):2696–2708.
33. Wang HL, Lai TW. Optimization of Evans blue quantitation in limited rat tissue samples. Sci Rep 2014;4:6588.
34. Hoffmann A, Bredno J, Wendland M, Derugin N, Ohara P, Wintermark M. High and low molecular weight fluorescein isothiocyanate (FITC)-dextrans to assess blood-brain barrier disruption: Technical considerations. Transl Stroke Res 2011;2(1):106–111.
35. Angell-Petersen E, Spetalen S, Madsen SJ, et al. Influence of light fluence rate on the effects of photodynamic therapy in an orthotopic rat glioma model. J Neurosurg 2006;104(1): 109–117.
36. Fingar VH. Vascular effects of photodynamic therapy. J Clin Laser Med Sur 1996;14(5):323–328.
37. Hu SS, Cheng HB, Zheng YR, Zhang RY, Yue W, Zhang H. Effects of photodynamic therapy on the ultrastructure of glioma cells. Biomed Environ Sci 2007;20(4):269–273.
38. Sporn LA, Foster TH. Photofrin and light induces microtubule depolymerization in cultured human endothelial cells. Cancer Res 1992;52(12):3443–3448.
39. Agostinis P, Berg K, Cengel KA, et al. Photodynamic therapy of cancer: An update. Ca-a Cancer J Clin 2011;61(4):250–281.
40. Kusama Y, Bernier M, Hearse DJ. Singlet oxygen-induced arrhythmias. Dose- and light-response studies for photoactivation of rose bengal in the rat heart. Circulation 1989;80(5):1432–1448.
41. Vandeplassche G, Bernier M, Thone F, Borgers M, Kusama Y, Hearse DJ. Singlet oxygen and myocardial injury: Ultrastructural, cytochemical and electrocardiographic consequences of photoactivation of rose bengal. J Mol Cell Cardiol 1990;22(3):287–301.

42. Yoshino F, Shoji H, Lee MCI. Vascular effects of singlet oxygen (O-1(2)) generated by photo-excitation on adrenergic neurotransmission in isolated rabbit mesenteric vein. Redox Rep 2002;7(5):266–270.
43. Ito S, Rachinger WH, Reulen HJ, Stummer W. Oedema formation in experimental photo-irradiation therapy of brain tumours using 5-ALA. Acta Neurochir 2005;147(1):57–65.
44. Westphal M. 5-aminolevulinic acid induced endogenous porphyrin fluorescence in 9L and C6 brain tumours and in the normal rat brain—Comment. Acta Neurochir 1998;140(5): 512–513.
45. Filippidis AS, Carozza RB, Rekate HL. Aquaporins in brain edema and neuropathological conditions. Int J Mol Sci 2017;18(1):55.
46. Michinaga S, Koyama Y. Pathogenesis of brain edema and investigation into anti-edema drugs. Int J Mol Sci 2015;16(5): 9949–9975.
47. Semyachkina-Glushkovskaya O, Chehonin V, Borisova E, et al. Photodynamic opening of the blood-brain barrier and pathways of brain clearing. J Biophotonics 2018;11:e201700287.
48. Semyachkina-Glushkovskaya O, Abdurashitov A, Dubrovsky A, et al. Application of optical coherence tomography for *in vivo* monitoring of the meningeal lymphatic vessels during opening of blood-brain barrier: Mechanisms of brain clearing. J Biomed Opt 2017;22(12):1.
49. Antila S, Karaman S, Nurmi H, et al. Development and plasticity of meningeal lymphatic vessels. J Exp Med 2017; 214(12):3645.
50. Johnston M, Zakharov A, Papaiconomou C, Salmasi G, Armstrong D. Evidence of connections between cerebrospinal fluid and nasal lymphatic vessels in humans, non-human primates and other mammalian species. Cerebrospinal Fluid Res 2004;1(1):1–13.
51. Gomez DG, Ehrmann JE, Gordon PD, Pavese AM, Gilanian A. The arachnoid granulations of the newborn human: An ultrastructural study. Int J Dev Neurosci 1983;1(2): 139–145.
52. Zhu D, Larin KV, Luo QM, Tuchin VV. Recent progress in tissue optical clearing. Laser Photonics Rev 2013;7(5): 732–757.
53. Zhao YJ, Yu TT, Zhang C, Li Z, Luo QM, Xu TH, Zhu D. Skull optical clearing window for *in vivo* imaging of the mouse cortex at synaptic resolution. Light: Sci Appl 2018;7:17153.
54. Stummer W, Stepp H, Wiestler OD, Pichlmeier U. Randomized, prospective double-blinded study comparing 3 different doses of 5-aminolevulinic acid for fluorescence-guided resections of malignant gliomas. Neurosurgery 2017;81(2): 230–239.
55. Stylli SS, Kaye AH, MacGregor L, Howes M, Rajendra P. Photodynamic therapy of high grade glioma—Long term survival. J Clin Neurosci 2005;12(4):389–398.
56. Dupont C, Mordon S, Deleporte P, Reyns N, Vermandel M. A novel device for intraoperative photodynamic therapy dedicated to glioblastoma treatment. Future Oncol 2017;13-(27): 2441–2454.